DFT Study of Cysteine Adsorption on Au(111)

Rosa Di Felice,*,†,‡ Annabella Selloni,‡ and Elisa Molinari†

Department of Chemistry, Princeton University, Princeton, New Jersey 08544, and INFM National Center for nanoStructures and bioSystems at Surfaces (S³) and Dipartimento di Fisica, Università di Modena e Reggio Emilia, Via Campi 213/A, Modena, Italy

Received: October 18, 2002

The adsorption of the cysteine amino acid ($H-SC_\beta H_2-C_\alpha H-NH_2-COOH$) on the (111) surface of gold is studied by means of periodic density functional calculations. Results for different adsorption sites and molecular configurations show that chemisorption involving S(thiolate)−Au bonds on Au(111) is favored by starting with either cysteine or cystine gas-phase molecular precursors. In the most stable adsorption configuration, the sulfur headgroup sits at the bridge site between two surface Au atoms, and the $S-C_\beta$ bond is tilted by 57° with respect to the surface normal, whereas the in-plane orientation of the molecular backbone plays a secondary role. The analysis of the electronic properties shows that the hybridization of the *p*-like S states with the *d*-like Au states produces both bonding and antibonding occupied orbitals, and the process is well described by a model for the interaction of localized orbitals with narrow-band dispersive electron states. The bonding orbitals well below the Fermi level contribute to the strong chemisorption of cysteine on gold. The calculated sulfur-projected density of states allows us to locate the cysteine molecular orbitals with respect to the system Fermi level, which gives a measure of the injection barrier at the molecule/electrode junction.

1. Introduction

Organic molecules and biomolecules with a sulfur headgroup are attracting considerable interest because of their wide use in nanotechnology-related fields, like surface patterning and functionalization[1,2] and molecular electronics.[3] Among the several interesting applications, the strong affinity of sulfur to different metals can be exploited to form contacts, to link other species to a supporting metallic surface, or to form well-ordered self-assembled monolayers (SAMs).[1] In biomolecules, the S-containing cysteine and cystine amino acids are especially interesting because, being often on the border of large proteins, they can provide a link to anchor these proteins to inorganic supports. For instance, experimental studies have found that a stable functional monolayer of *Pseudomonas Aeruginosa* azurin can be formed on Au(111)[4] and also on a functionalized SiO_2[5,6] substrate by attaching the protein to the surface via its Cys3-Cys26 disulfide group.

Recently, cysteine and cystine moleules have been deposited on different gold surfaces to form ordered layers[7,8] and wires.[9] In particular, highly ordered and stable monolayers showing the same two-dimensional (2D) periodicity and structure, have been obtained on an Au(111) electrode in aquaeous solution.[7] However, the character of the molecule-surface bonding, notably the question whether this involves adsorbed thiolate or disulfide species, remained unclear. This question is a long-standing one in the context of SAMs formed by alkanethiols on Au(111).[10] Recent first principles calculations[11−14] generally support the thiolate solution, but many experimental results still remain which are best explained by the occurrence of disulfide bonds.[10]

In view of this controversial situation, and also because of the special importance of the thiolate vs disulfide issue in the case of proteins, whose stability and functionality may be influenced by the breaking of the disulfide bond[4] when they are attached to substrates, in this paper, we use first-principle plane-wave pseudopotential density functional theory (DFT) calculations to directly study the adsorption geometry and bonding properties of cysteine on Au(111), without relying on previous theoretical results for alkanethiols. In this way, we shall also be able to study the influence of the molecular backbone on the adsorption properties. We shall assume that the molecules are in their neutral (gas-phase) configuration, and also restrict our exploration of possible adsorption structures to configurations where the molecules are bonded to the surface only via their sulfur headgroups. These geometries are relevant to high-density monolayers on close-packed surfaces, for which two-point configurations, where cysteine is attached to the surface both via the strong S−Au bond and the weaker bond involving the lone-pairs on the amino groups,[9,15] become unlikely. Whereas most of our calculations refer to cysteine, preliminary results for cystine on Au(111) are also presented, which further support a thiolate-like adsorption.

2. Computational Approach

The unreconstructed 1×1 structure was considered for the Au(111) surface, since the $(\sqrt{3} \times 23)$ herringbone reconstruction[16] is known to be lifted upon molecular chemisorption.[17] To model the surface we used a slab of four Au layers (three Au layers to treat the case of cystine adsorption, see details in section 4), with a periodically repeated $(2\sqrt{3} \times 3)$ 2D supercell, corresponding to a surface area of 10.14×8.78 Å^2, and including 12 Au atoms per layer. One cysteine molecule, adsorbed on the upper surface of the slab, was present in each $(2\sqrt{3} \times 3)$ cell. The density of adsorbed molecules in our calculations is about half the experimental density for "wet" monolayers,[7] where a $(3\sqrt{3} \times 6)$R30 unit cell containing six cysteine (three cystine) molecules was observed.

* To whom correspondence should be addressed. Phone: +39-059-2055301. Fax: +39-059-374794. E-mail rosa@unimore.it.
† INFM-S³ and Università di Modena e Reggio Emilia.
‡ Princeton University.

10.1021/jp0272421 CCC: $25.00 © 2003 American Chemical Society
Published on Web 12/19/2002

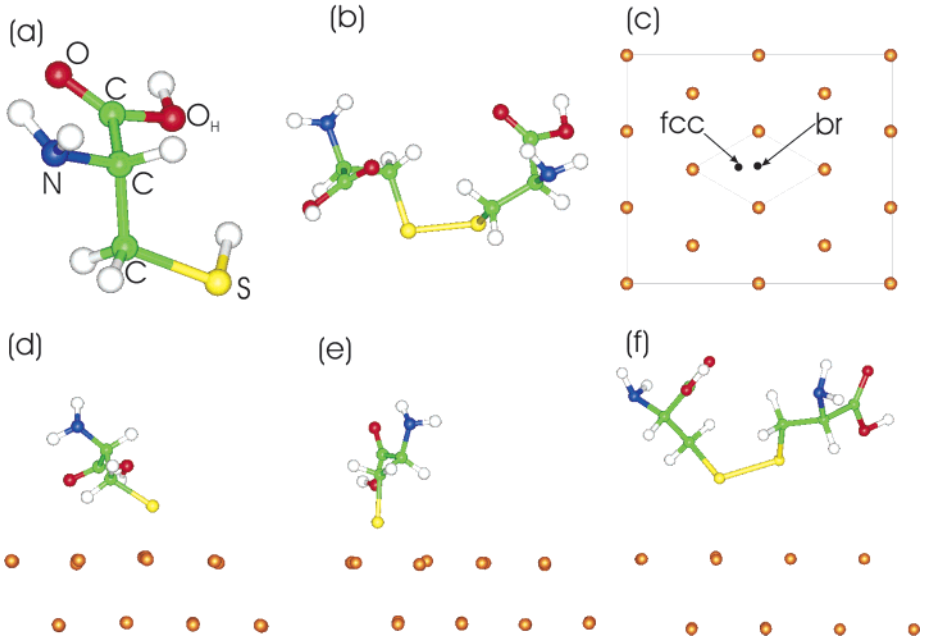

Figure 1. Relaxed atomic structure of the free and chemisorbed molecules. (a) Free cysteine molecule, with indication of the atomic species as used in the text and tables; (b) free cystine molecule; (d) cys• chemisorbed on Au(111) with S_γ at he bridge site, and the $S_\gamma-C_\beta$ bond tilted with respect to the surface normal; (e) cys• chemisorbed on Au(111) with S_γ at the hollow fcc site, and the $S_\gamma-C_\beta$ bond parallel to the surface normal; (f) molecular (nondissociative) adsorption configuration of cystine on Au(111). In (c) a top view of the $2\sqrt{3} \times 3$ supercell is shown, with indication of the adsorption sites for the cysteine S headgroup. Orange, yellow, white, blue, red, and green spheres represent Au, S, H, N, O, and C atoms, respectively.

Calculations have been performed in the frame of DFT, using the gradient-corrected PW91 exchange-correlation functional.[18−19] Electron−ion interactions have been described by ultrasoft pseudopotentials[20] for all of the species except S, for which a norm-conserving Troullier and Martins[21] pseudopotential was used. The electron wave functions were expanded in a plane wave basis with a kinetic energy cutoff of 22 Ry. This was found sufficient to yield a converged value of the bond length for the diatomic N_2 and O_2 molecules (generally difficult to describe in plane waves). The Brillouin zone (BZ) sums were calculated including 4 Monkhorst-Pack special **k** points[22] in the irreducible wedge. All of the atomic positions were relaxed until the forces vanished within 0.05 eV/Å. Further details and tests have been described in an earlier study of methanethiols on Au(111).[14]

3. Calculations for Gas-Phase Species

To validate the accuracy of our approach, we first examined the properties of cysteine and cystine in the gas phase.[23] For cysteine, we take a conformation which is slightly higher in energy (by only 0.3 kcal/mol) than the one predicted to be the most stable by high level MP2 calculations[23b] but which is structurally more similar to the conformations observed in molecular cysteine crystals.[24] In particular, the torsion angles that we obtain for the other conformation[23b] are not consistent with the X-ray structure.[24] In Figure 1a(1b) we show the equilibrium structure obtained for cysteine (cystine), with the definition of the atomic labels. In Table 1, the computed equilibrium bond distances and angles for cysteine are reported and compared to X-ray data[24] (in parentheses) for a monoclinic crystal with two cysteine molecules per unit cell. The agreement of our results with the X-ray data as well as with the results of quantum chemistry calculations[25] is quite good: the bond lengths and angles have an average accuracy of 2%, the only notable exceptions being the $C-O_H$ distance (9%) and the $C_\alpha-C-O$ angle (6%). These larger deviations are most likely related to the fact that in the crystal the protons of carboxylic groups are largely transferred to neighboring amino groups through intermolecular O···H−N hydrogen bonds.[24] However, although the detailed state of the tailgroup may affect lateral intermolecular interactions, it should not compromise the analysis of the local Au−S chemical bonding, which is the main target of our investigation. For the cystine molecule, the calculated S−S distance is 2.12 Å, the torsion angle between the two $C_\beta S$ bonds is 78°, and the structure of the two cysteine fragments in the disulfide remains very similar to that of isolated cysteine.

TABLE 1: Structure of the Gas-Phase Cysteine Molecule (2nd Column) and of the Adsorbed Cysteine Radical (3rd and 4th Columns)[a]

	Cys	Cys•$_{br}$/Au(111)	Cys•$_{fcc}$/Au(111)
	Bond Distance (Å)		
$N-C_\alpha$	1.47 (1.49)	1.47	1.46
C_α-C	1.52 (1.53)	1.53	1.53
C−O	1.23 (1.26)	1.23	1.22
$C-O_H$	1.37 (1.25)	1.36	1.36
$C_\alpha-C_\beta$	1.55 (1.53)	1.54	1.55
$C_\beta-S_\gamma$	1.86 (1.81)	1.88	1.90
	Bond Angle (°)		
$C-C_\alpha-C_\beta$	111.3 (111.6)	109.5	112.1
$C-C_\alpha-N$	109.1 (109.9)	112.4	109.3
C_β-$C_\alpha-N$	109.3 (109.3)	107.0	107.5
$C_\alpha-C-O$	124.6 (118.1)	123.3	124.3
$C_\alpha-C-O_H$	113.1 (116.2)	113.1	112.0
$C_\alpha-C_\beta-S_\gamma$	116.8 (114.4)	114.2	116.5
$O-C-O_H$	122.3 (125.7)	123.6	123.7
	Torsion Angle (°)		
$C_\beta-C_\alpha-C-O$	116.9	71.5	115.4
$Cb-C_\alpha-C-O_H$	−62.4	−108.0	−64.6
$S_\gamma-C_\beta-C_\alpha-N$	−155.9	−168.6	−159.5
$S_\gamma-C_\beta-C_\alpha-C$	83.5	69.2	80.5
$N-C_\alpha-C-O$	−3.8	−47.3	−3.7
$N-C_\alpha-C-O_H$	176.9	133.0	176.4

[a] The values in parenthesis for free cysteine are experimental X-ray data.[24] The atomic labels are indicated in Figure 1A.

Next, we consider the energies of the RS−H and of the RS−SR bonds (with the residue R being COOH−NH_2−HC−H_2C in our case). We find $E_{S-S} = 68.6$ kcal and $E_{S-H} = 89.5$ kcal for the RS−SR and the RS−H bonds, respectively, in good agreement with the experimental[26] (theoretical[12]) estimates of $E_{S-S} = 65(72)$ kcal/mol and $E_{S-H} = 86(91)$ kcal/mol obtained for methanethiol and dimethyl disulfide (with the residue R being CH_3).

Finally, we can evaluate the gas-phase energetics and obtain reference values for the calculation of the chemisorption energies on the metal surface. Dissociation of cysteine into a cysteine radical (hereafter denoted cys•) and molecular hydrogen, i.e. 2cysteine → 2cys• + H_2, is found to be endothermic by 75 kcal/mol, whereas dissociation of cystine into cysteine in the presence of molecular hydrogen (cystine + H_2 → 2cysteine) is exothermic by 6.3 kcal/mol. The latter energy gain upon dissociation of cystine indicates a tendency toward the breaking of the disulfide bridge, in an ambient where the S atoms are able to form new stronger bonds. Similarly to the formation of S−H bonds in the presence of hydrogen, in the following, we show that in the presence of a reactive Au surface, S−Au bonds are formed at the expense of disulfide breaking.

4. Results and Discussion

It is widely accepted that on the Au(111) surface the S−H bonds of thiol molecules dissociate to yield S(thiolate)−Au bonds.[1,10,12] Moreover, recent theoretical studies have found that the preferential adsorption site for the S headgroup is the bridge site[13,14,27] (slightly displaced toward an fcc location), followed by the fcc hollow site, whereas the hcp and on-top sites are less favorable. Assuming a similar behavior for cysteine, we have examined cys• adsorption configurations with the S headgroup at the energetically most favorable bridge and fcc sites (see Figure 1c). More precisely, we considered four different configurations, two structures with the S headgroup at the bridge site and two structures with the S headgroup at the fcc site. At each adsorption site, two structures with a different orientation of the molecular backbone with respect to the surface lattice were computed. Thus, we took into account the effect of the tailgroup anisotropy into the determination of the equilibrium geometry. For the adsorption at the bridge site, we started with the $S_\gamma-C_\beta$ bond tilted by 60° with respect to the surface normal, whereas for the adsorption at the fcc site, we started with the $S_\gamma-C_\beta$ bond along the surface normal. Calculations were done using a slab of four Au layers, and all of the atoms were free to relax in the structural optimization procedure.

Analogous calculations were done for one possible adsorption geometry of cystine/Au(111), starting from a configuration where the two S atoms of the disulfide bonds are approximately on top of two nearest neighbor surface Au atoms, as suggested for dimethyl disulfide on Au(111).[12] To make the calculations more manageable, however, for cystine, we reduced the number of layers in the gold slab from four to three. To be able to compare the relative stability of cysteine (thiolate) vs cystine (disulfide) adsorption, the most stable adsorption structure for cysteine was then recalculated using the thinner slab. However, the comparison is not strict because in our calculations the packing of adsorbed cystine molecules is denser than that of cysteine, which may give rise to different lateral interactions between adsorbed molecules in the two cases.

4.1. Structure. The relaxed geometries for the lowest energy structure of the cysteine radical at the bridge and fcc sites are shown in Figure 1, parts d and e, respectively, whereas the calculated structural parameters are reported in Tables 1 and 2.[28] The internal conformation of the adsorbed radical is slightly affected by the adsorption process, with the only exception being the torsion angles involving the carboxyl and amino groups for the adsorption at the bridge site (compare the second and third columns in Table 1). We attribute the large variation of the torsion angles, with respect to the free molecule, to the effect of steric molecule−substrate interactions. This is consistent with the fact that at the fcc site, where the two functional groups NH_2 and COOH are far away from the surface, the torsion angles do not change significantly with respect to the free molecule (compare the second and fourth columns in Table 1).

TABLE 2: Parameters of the Adsorption Geometries for Cys•/Au(111)[a]

	bridge site	Fcc site
Δz (Å)	0.25	0.15
h_S (Å)	2.07	1.63
d_{S-Au} (Å)	2.51	2.51
Θ (°)	57	3

[a] Δz is the corrugation in the top gold layer; h_S is the height of the cys• S atom above the substrate; d_{S-Au} is the nearest-neighbor S−Au distance. Θ is the angle formed by the $S_\gamma-C_\beta$ bond with the surface normal.

We find significant differences in the thiolate adsorption geometries at the two sites: the height of the molecule above the surface plane (h_S in Table 2), for instance, changes from 2.1 Å at the bridge location to 1.6 Å at the fcc location, and the tilt angle with respect to the surface normal changes from 57° to 3°. Instead, the S−Au distance is unaffected, despite the fact that S has a different number of Au nearest neighbors in the two different configurations: 2 at the bridge site and 3 at the fcc site. The structural parameters that we obtain for cys•/Au-(111) are close to previous determinations of the equilibrium geometry of SCH_3/Au(111): for instance, we find that the S−Au distance is 2.51 Å, which compares very well with the S−Au distance reported for the thiols[13] at the bridge (2.50 Å) and at the fcc (2.52 Å) sites of Au(111). The same agreement is found for the tilt angle.[13−14]

For cystine, an equilibrium molecular adsorbed state is found (see Figure 1f), in which the S−S dimer bond length is 2.15 Å, practically identical to that of the isolated cystine (see section 3). Even though we started with the S−S dimer flat above the surface, in the final optimized configuration, the dimer is buckled by as much as 0.62 Å. For the lower (upper) S atom of the disulfide bridge, the distances from the two "bridging" Au atoms are 2.86 (3.48) and 3.45 Å (4.04 Å), significantly larger than in the case of thiolate chemisorption. During our relaxation procedure, we also observed a large lateral displacement of the dimer with respect to the underlying Au(111) lattice, which seems driven by a tendency of the S atoms to approach the bridge sites. This tendency is counterbalanced by the lateral repulsion between H atoms of cystine molecules in neighboring (replicated) cells, and the two opposing factors determine the equilibrium geometry. However, a more comprehensive phase space sampling, including different molecular coverages and different initial configurations, will be needed to attain a more complete understanding of the molecular adsorption state.

4.2. Energetics. In Table 3, our results for the stability of the investigated adsorption configurations are summarized. For the case of thiolate adsorption, we found that rotation selectivity due to the tailgroup anisotropy gives a negligible energy variation at the fcc site, and an energy variation of 2.4 kcal per adsorbed radical at the bridge site, which does not affect the energy balance between the two inequivalent adsorption sites.

TABLE 3: Formation Energies (kcal/mol) with Respect to Free Cysteine (E_1) and Cystine (E_2) Molecules, and Clean Au(111), According to the Reactions Explicitly Indicated[a]

system	E_1	E_2
cysteine	0	−6.3 (cystine+H_2→2cysteine)
cystine	+6.3 (2cysteine→cystine+H_2)	0
cys•	+75.0 (2cysteine→2cys•+H_2)	+68.6 (cystine→2cys•)
Cys•$_{br}$/Au(111)	−19.4 2[Au(111)+cysteine]→2cys•$_{br}$/Au(111)+H_2	−25.8 (−31) 2Au(111)+cystine→2cys•$_{br}$/Au(111)
Cys•$_{fcc}$/Au(111)	−11.1 2[Au(111)+cysteine]→2cys•$_{fcc}$/Au(111)+H_2	−17.4 2Au(111)+cystine→2cys•$_{br}$/Au(111)
Cystine/Au(111)	-	(−17) Au(111)+cystine→cystine/Au(111)

[a] Values in parenthesis have been obtained using a Au(111) slab of three layers.

Therefore, in Table 3, only the lowest energy structure for each of the two inequivalent sites is included. E_1 denotes the formation energy with respect to cysteine molecules with H_2 evaporation, whereas E_2 is the formation energy with respect to cystine molecules, as it clearly appears from the chemical reactions reported in Table 3.

The values in Table 3 show that thiolate adsorption on Au(111) is energetically favorable (exothermic) starting from either cysteine or cystine in the gas-phase; that is, both the cysteine S−H bond and the cystine disulfide S−S bond are predicted to be cleaved in the vicinity of the (111) surface of gold. In addition, the adsorption is a site-selective process, because the bridge site is more stable by 8.3 kcal/mol with respect to the fcc hollow site. The energy gain for the most favorable thiolate configuration is 25.8 (31) kcal/mol,[29] with respect to free cystine and clean Au(111), using the Au slab with four (three) layers. Such a strong exothermicity already suggests that in the vicinity of an Au(111) surface cystine is likely to dissociate and give origin to thiolate S−Au bonds. This indication is further supported by the large difference in the energy E_2 for the cys•$_{br}$/Au(111) system and for the molecular (undissociated) cystine configuration using the slab of three layers (see Table 3). Even though our sampling of possible adsorption configurations is quite limited, especially for the case of cystine, it seems safe to conclude that dissociative adsorption is largely favored, at least under dry conditions. In fact, despite the fact that a more favorable configuration might be found for the disulfide adsorption state, it is unlikely that the adsorption energy may increase by more than 14 kcal/mol, as it would be needed to overcome the thiolate adsorption.

4.3. Electronic Properties. We now analyze the electronic features of the molecule/surface bond, focusing on the most favorable S(thiolate)−Au configuration, with the S headgroup at a bridge site.

In the lower panel of Figure 2, the total density of states (DOS) of the system cys•$_{br}$/Au(111) is shown (solid curve), with the Fermi level set as the origin of the energy scale. The DOS of the clean Au(111) surface is shown as a dotted curve. The plot is limited to the energy range where the Au valence states are present. At lower energies, the valence electron states are fully localized on the adsorbed radical, and no substrate−adsorbate interaction is present; that is, the states maintain the same character as in isolated cysteine. The band extending from about 2 to 6 eV below the Fermi level is characteristic of the Au *d* orbitals.[30] The differences between the clean and the cysteine-covered Au(111) surfaces, shown by the inequivalence of the solid and dotted curves in Figure 2 (bottom), are due to the substrate−adsorbate interactions. In the insets, isosurface plots of the charge density of S-localized *p*-like orbitals are shown for the *isolated* cysteine radical: these are the electron states that interact with the delocalized Au states to form hybrid orbitals in the cys•-covered gold surface. The states at −1.1 eV are two degenerate HOMOs of the isolated radical.

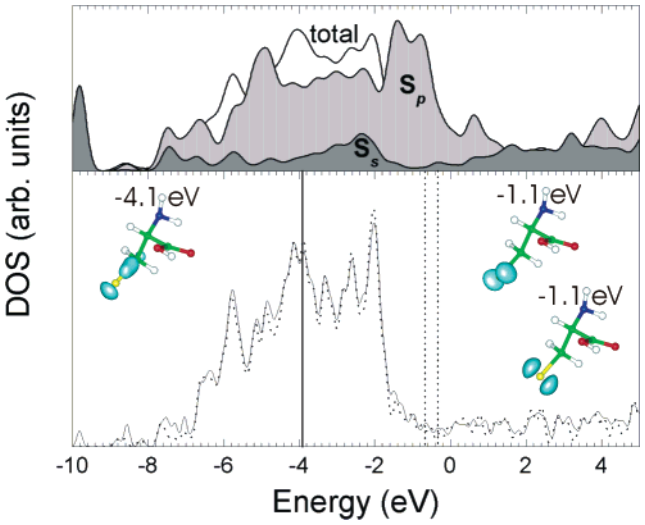

Figure 2. Bottom panel: Density of States of the Au(111) surface with an adsorbed cysteine radical per $2\sqrt{3} \times 3$ cell (solid curve) and of the clean unreconstructed Au(111) surface (dotted curve). The solid (dotted) vertical lines identify the energy positions of the selected hybrid bonding (antibonding) S−Au orbitals shown in Figure 3. The Fermi level has been set as the origin of the energy scale. The insets show charge density plots of the S-localized orbitals of the isolated cysteine radical and the corresponding energy levels are indicated (on the same energy scale used for the DOS). Top panel: the *s* and *p* S-projected DOS of the system cys•$_{br}$/Au(111) are shown as the dark gray and light gray area, respectively, and superimposed to the total DOS (white area). The comparison between the total DOS for the clean and for the cysteine-covered Au(111) surface in the bottom panel is made by aligning the Fermi energies from the two calculations. The assignment of the free radical energy levels on the scale of the DOS and SPDOS is achieved by aligning the deepest level (identical for the free and adsorbed radical) from the calculations for cys• and for cys•$_{br}$/Au(111), localized at the COOH group.

In the top panel of Figure 2, the sulfur-projected DOS (SPDOS) is shown in comparison with the total DOS: the light (dark) gray area refers to the projection on *p* (*s*) orbitals of S, whereas the white area emerging from the shaded areas is the total DOS. This comparison allows us to get a deeper insight into the S−Au interaction. The *p* SPDOS exhibits pronounced peaks above and below the Au *d* band. This is in agreement with the Newns-Anderson model for atomic and molecular chemisorption on metal surfaces, which predicts that the interaction of a localized orbital on the adsorbate with the narrow *d* band of the metal produces hybrid orbitals of both bonding

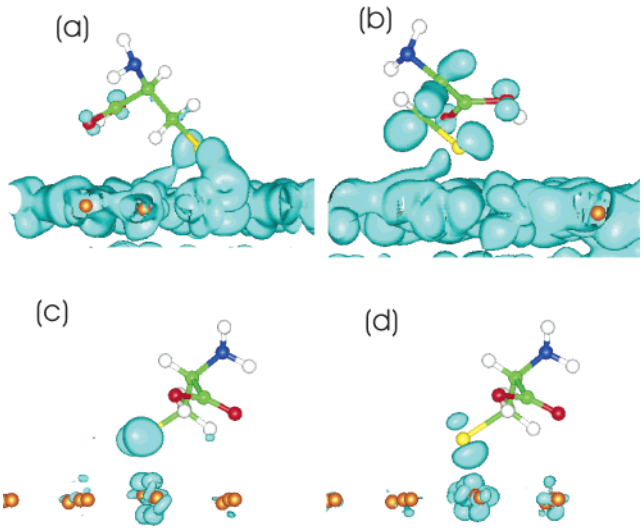

Figure 3. Isosurfaces of representative bonding and antibonding orbitals resulting from S−Au hybridization. (a) π-like bonding orbital at $E = -3.86$ eV; (b) σ-like bonding orbital at $E = -3.85$ eV; (c) π-like antibonding orbital at $E = -0.64$ eV; (d) σ-like antibonding orbital at $E = -0.34$ eV. The energies are expressed relative to the system Fermi level.

and antibonding type, below and above the center of the metal *d* band, respectively.[30] In our case, the S−Au antibonding orbitals resulting from the hybridization of the cys• HOMO (right insets in the bottom panel of Figure 2) with the Au *d* band give rise to the upper peak in the *p* SPDOS, centered at about −1 eV. The corresponding S−Au bonding orbitals contribute both to the broad band which is spread throughout the metal *d* band and to the lower peak in the *p* SPDOS. The latter peak, centered at about −5 eV, includes also the interaction of the Au electron states with the deep-level cys• orbital shown in the left inset in the bottom of Figure 2. Thus, the complete *p* SPDOS results from the interaction of all of the three *p*-like orbitals of the isolated radical with the Au atoms.

The above interpretation is supported by an analysis of the one-particle electron states, which reveals the formation of S−Au bonding and antibonding orbitals of both π-like and σ-like character below the Fermi level. In Figure 3, in particular, we show isosurface plots of orbitals originating from the hybridization of the cys• HOMOs with the Au *d* band, and the energetic positions of these states are indicated by vertical lines (solid and dashed for the bonding and antibonding states, respectively) in the bottom panel of Figure 2. The interaction of the deep radical level at −4.1 eV with the Au *d* band gives rise to hybrid orbitals (not shown here) with energy ranging from −5.5 to −4.5 eV. The state represented in Figure 3a (3b) is a π-like (σ-like) bonding orbital at the energy −3.86 eV (−3.85 eV) relative to the Fermi level, resulting from the hybridization of the radical's HOMO with the Au *d* states: other similar bonding orbitals appear with energies in the range $-5.6 \div -4.5$ eV ($-5.5 \div -4.7$ eV). In synthesis, the energy range between −5.5 and −4.5 eV defining the lower peak in the S_p SPDOS, is characterized by both π-like and σ-like S−Au bonding electron states. The state represented in Figure 3c (3d) is the analogous π-like (σ-like) antibonding orbital at the energy −0.64 eV (−0.34 eV) relative to the Fermi level. The presence of both bonding and antibonding occupied states weakens the Au−S interaction with respect to a complete bonding picture. However, the presence of empty antibonding Au−S(HOMO) electron states above the Fermi level (see the SPDOS in Figure 2) suggests that the bonding contribution resulting from the hybridization with the *d* bands is not canceled out completely in this case.[30] The downward shift of the HOMO bonding energy level (from −1.1 eV for the isolated cys• to the −5 eV peak for the adsorbed cys•) is substantially larger than the upward shift of the HOMO antibonding level (from −1.1 eV to −1 eV).

The molecular LUMO, at about 4 eV above the HOMO, is localized on the COOH group and does not show any hybridization with the metal electron states.

5. Summary

In this paper, we have examined the chemisorption of cysteine on the Au(111) surface, on the basis of DFT-PW91 calculations of the adsorption geometries and of the electronic properties. Our results show that the adsorption involves S(thiolate)−Au bonds, with the S headgroups sitting preferentially at bridge sites. Although the energetic trends are qualitatively similar to those for methanethiol and dimethyl disulfide on Au(111),[13−14,27] indicating that the molecular backbone does not influence the local structural and electronic details of the Au−S bonding and the choice for the stable adsorption site, the complex tailgroup of cysteine appears to have an important role in the quantitative determination of the adsorption energy (this becomes clear from an explicit comparison of the values in Table 3 with those reported by Vargas and co-workers[14]).

The investigation of the electronic DOS for the most stable adsorption configuration shows peaks due to the hybridization between the S *p* orbitals and the Au *d* band: in particular, the bonding peak is located at 5 eV below the Fermi level, and the antibonding peak is located at 1 eV below the Fermi level. To our knowledge, this is the first detailed analysis of the S(thiolate)−Au hybrid orbitals.

Our results provide a deeper insight into the role played by S headgroups in the attachment of molecules to metallic substrates and leads. Besides providing the energetics of different adsorption reactions, they show the modified energy levels of the molecules and allow to determine the lineup between the molecular HOMO with respect to the metal Fermi level: this information is crucial for the interpretation of transport phenomena in molecular electronic devices.[31] It emerges that the Fermi level cannot be simply placed in the middle of the HOMO−LUMO gap but depends on the interface bonding features. Despite the fact that our study quantitatively applies to cysteine, many qualitative features may be extended to other molecular systems where the highest occupied energy levels are associated to a S atom.

Acknowledgment. Our research was funded by the EU under Project SAMBA and by INFM through PRA-SINPROT. Computer time was provided by the INFM Parallel Computing Committee through grants for parallel supercomputing at CINECA (Bologna, Italy) and by the Princeton Materials Institute. We are grateful to M.G. Betti, F. De Rienzo, P. Facci, and G. Scoles for scientific discussions.

References and Notes

(1) Ulman, A. *Chem. Rev.* **1996**, *96*, 1533.
(2) Xia, Y.; Rogers, J. A.; Paul, K. E.; Whitesides, G. M. *Chem. Rev.* **1999**, *99*, 1823.
(3) Joachim, C.; Gimzewski, J. K.; Aviram, A. *Nature* **2000**, *408*, 541.
(4) Chi, Q.; Zhang, J.; Nielsen, J. U.; Friis, E. P.; Chorkendorff, I.; Canters, G. W.; Andersen, J. E. T.; Ulstrup, J. *J. Am. Chem. Soc.* **2000**, *122*, 4047.
(5) Rinaldi, R.; Biasco, A.; Maruccio, G.; Cingolani, R.; Alliata, D.; Andolfi, L.; Facci, P.; De Rienzo, F.; Di Felice, R.; Molinari, E. *Adv. Mater.* **2002**, *14*, 1453.

(6) Facci, P.; Alliata, D.; Andolfi, L.; Shnyder, B.; Koetz, R. *Surf. Sci.* **2002**, *504*, 282. Andolfi, L.; Facci, P. unpublished.

(7) Zhang, J.; Chi, Q.; Nielsen, J. U.; Friis, E. P.; Andersen, J. E. T.; Ulstrup, J. *Langmuir* **2000**, *16*, 7229.

(8) Dakkouri, A. S.; Kolb, D. M.; Edelstein-Shima, R.; Mandler, D. *Langmuir* **1996**, *12*, 2849. Xu, Q.-M.; Wan, L.-J.; Wang, C.; Bai, C.-L.; Wang, Z.-Y.; Nozawa, T. *Langmuir* **2001**, *17*, 6203.

(9) Kühnle, A.; Linderoth, T. R.; Hammer, B.; Besenbacher, F. *Nature* **2002**, *415*, 891.

(10) Poirier, G. E. *Chem. Rev.* **1997**, *97*, 1117. Schreiber, F. *Prog. Surf. Sci.* **2000**, *65*, 151.

(11) Hakkinen, H.; Barnett, R. N.; Landman, U. *Phys Rev. Lett.* **1999**, *82*, 3264.

(12) Grönbeck, H.; Curioni, A.; Andreoni, W. *J. Am. Chem. Soc.* **2000**, *122*, 2839.

(13) Hayashi, T.; Morikawa, Y.; Nozoye, H. *J. Chem. Phys.* **2001**, *114*, 7615.

(14) Vargas, M. C.; Giannozzi, P.; Selloni, A.; Scoles, G. *J. Phys. Chem. B* **2001**, *105*, 9509.

(15) Sljivancanin, Z.; Gothelf, K. V.; Hammer, B. to be published.

(16) Sandy, A. R.; Mochrie, S. G.; Zehner, D. M.; Huang, K. G.; Gibbs, D. *Phys. Rev. B* **1991**, *43*, 4667.

(17) Poirier, G. E.; Pylant, E. D. *Science* **1996**, *272*, 1145. Kondoh, H.; Kodama, C.; Sumida, H.; Nozoye, H. *J. Chem. Phys.* **1999**, *111*, 1175.

(18) Perdew, J. P.; Chevary, J. A.; Vosko, S. H.; Jackson, K. A.; Singh, D. J.; Fiolhais, C. *Phys. Rev. B* **1992**, *46*, 6671.

(19) We used the code PWSCF by Baroni, S.; Dal Corso, A.; de Gironcoli, S.; Giannozzi, P., available at http://www.pwscf.org.

(20) Vanderbilt, D. *Phys. Rev. B* **1990**, *41*, 7892.

(21) Troullier, N.; Martins, J. L. *Phys. Rev. B* **1992**, *46*, 1754.

(22) Monkhorst, H. J.; Pack, J. D. *Phys. Rev. B* **1976**, *13*, 5188.

(23) (a) Niehaus, T. A.; Elstner, M.; Frauenheim, Th.; Suhai, S. *J. Mol. Struct. (THEOCHEM)* **2001**, *541*, 185. (b) Gronert, S.; O'Hair, R. A. J. *J. Am. Chem. Soc.* **1995**, *117*, 2071.

(24) Görbitz, C. H.; Dalhus, B. *Acta Crystallogr. C* **1996**, *52*, 1756.

(25) Hameka, H. F.; Jensen, J. O.; Ong, K. K.; Samuels, A. C.; Vlahacos, C. P. *J. Phys. Chem. A* **1998**, *102*, 361.

(26) Nicovic, J. M.; Kreutter, K. D.; van Dijk, C. A.; Wine, P. H. *J. Phys. Chem.* **1992**, *96*, 2518.

(27) Gottschalk, J.; Hammer, B. *J. Chem. Phys.* **2002**, *116*, 784.

(28) The structural parameters h_S, d_{S-Au}, and Θ are the same for the two inequivalent tailgroup rotation geometries at each adsorption site.

(29) Although decreasing the slab thickness from four to three Au layers brings an error of 5 kcal/mol in the evaluation of absolute adsorption energies, the relative adsorption energies (between the thiolate and disulfide forms in our case) are more accurate by about an order of magnitude.

(30) Hammer, B.; Nørskov, J. K. In *Theory of Adorption and Surface Reactions*, in *Chemisorption and Reactivity of Supported Clusters and Thin Films*; Lambert, R. M., Pacchioni, G., Eds.; Kluwer Academic Publishers: The Netherlands, 1997.

(31) Xue, Y.; Datta, S.; Ratner, M. A. *J. Chem. Phys.* **2001**, *115*, 4292.